A FFT-BASED NUMERICAL METHOD FOR COMPUTING THE MECHANICAL PROPERTIES OF COMPOSITES FROM IMAGES OF THEIR MICROSTRUCTURES

H. MOULINEC, P. SUQUET
LMA/CNRS
31 Chemin Joseph Aiguier
13402. Marseille. Cedex 20. FRANCE

Abstract: The effective properties of composite materials are strongly influenced by the geometry of their microstructures, which can be extremely complex. Most of the numerical simulations known to the authors make use of two- or three-dimensional finite elements analyses which are often time consuming because of the complexity imposed by the requirement of extremely precise description of the reinforcements distribution. A numerical method is presented here that directly uses images of the microstructure - supposed to be periodically repeated - to compute the composite overall properties, as well as the local distribution of stresses and strains, without requiring further geometrical interpretation by the user. The linear elastic problem is examined first. Its analysis is based on the Lippmann-Schwinger's equation, which is solved iteratively by means of the Green operator of an homogeneous reference medium. Then the method is extended to non-linear problems where the local stress strain relation is given by an incremental relation.

Introduction

This study is devoted to a new numerical technique to compute the local and overall response of a nonlinear composite from *images* of its *real microstructure*. The need for developing these numerical simulations is twofold.

First, numerous studies have been devoted to nonlinear cell calculations using the Finite Element Method (FEM) and a list of comprehensive references (by no means exhaustive) include Adams and Donner (1967), Christman *et al* (1989), Tvergaard (1990), Brockenborough *et al* (1991), Böhm *et al* (1993), Michel and Suquet (1993), Nakamura and Suresh (1993). But the difficulties due to meshing and the large number of d.o.f.'s required by the analysis limit the complexity of the microstructures which can be investigated by means of the FEM.

The present method avoids the first difficulty (meshing), and makes use of fast Fourier transforms (FFT) to solve the unit cell problem, even in a nonlinear context. FFT algorithms require data sampled in a grid of regular spacing, allowing to use directly digital images of the microstructure. The second difficulty (size of the problem) is partially overcome by the use of an iterative method which does not require the formation of a stiffness matrix.

R. Pyrz (ed.), IUTAM Symposium on Microstructure-Property Interactions in Composite Materials, 235–246.

Second, the interest for numerical simulations of the nonlinear response of composites has recently been strengthened by the emergence of theoretical methods to predict analytically the nonlinear overall behavior of composites (Willis (1991), Ponte Castañeda (1992), Suquet (1993)). Part of the present study intends to give precise numerical results for uniaxial or multiaxial loading paths which could serve as guidelines for theoretical predictions.

1. Description of the method.

1.1. BOUNDARY CONDITIONS

The overall behavior of a composite is governed by the individual behavior of its constituents and by its microstructure. Its effective response to a prescribed path of macroscopic strains or stresses may be determined numerically via the resolution of the so-called "local problem" on a representative volume element (r.v.e.) V. In this study, the "representative" information on the microstructure is provided by an image (micrograph) of the microstructure of the composite of arbitrary complexity. The image contains $M \times N$ pixels and independent mechanical properties are assigned individually to each pixel.

The local problem consists in equilibrium equations, constitutive equations, boundary and interface conditions. All different phases are assumed to be perfectly bonded (hence displacements and tractions are continuous across interfaces). However, the displacements and tractions along the boundary of the r.v.e. are left undetermined and the local problem is ill-posed. We choose to close the problem with periodic boundary conditions which can be expressed as follows. The local strain field $\boldsymbol{\varepsilon}(\mathbf{u}(\mathbf{x}))$ is split into its average $\mathbf{E}$ and a fluctuation term $\boldsymbol{\varepsilon}(\mathbf{u}^*(\mathbf{x}))$:

$$\boldsymbol{\varepsilon}(\mathbf{u}(\mathbf{x})) \;=\; \boldsymbol{\varepsilon}(\mathbf{u}^*(\mathbf{x})) + \mathbf{E} \quad \text{or equivalently} \quad \mathbf{u}(\mathbf{x}) = \mathbf{u}^*(\mathbf{x}) + \mathbf{E}.\mathbf{x}$$

By assuming periodic boundary conditions it is assumed that the fluctuating term $\mathbf{u}^*$ is periodic (notation: $\mathbf{u}^*$ #), and the traction $\boldsymbol{\sigma}.\mathbf{n}$ is anti-periodic in order to meet the equilibrium equations on the boundary (notation: $\boldsymbol{\sigma}.\mathbf{n}$ $-$ #).

1.2. PRELIMINARY PROBLEM.

First, the preliminary problem of an homogeneous linear elastic body, with stiffness $\mathbf{c}^0$, subject to a polarization field $\boldsymbol{\tau}(\mathbf{x})$, is considered

$$\left.\begin{aligned} \boldsymbol{\sigma}(\mathbf{x}) = \mathbf{c}^0 : \boldsymbol{\varepsilon}(\mathbf{u}^*(\mathbf{x})) \;+\; \boldsymbol{\tau}(\mathbf{x}) \quad \forall \mathbf{x} \in V \\ \mathbf{div}\boldsymbol{\sigma}(\mathbf{x}) = \mathbf{0} \quad \forall \mathbf{x} \in V, \quad \mathbf{u}^* \;\#,\; \boldsymbol{\sigma}.\mathbf{n} \;-\; \# \end{aligned}\right\} \tag{1.1}$$

The solution of (1.1) can be expressed in real and Fourier spaces, respectively, by means of the periodic Green operator $\boldsymbol{\Gamma}^0$ associated with $\mathbf{c}^0$:

$$\boldsymbol{\varepsilon}(\mathbf{x}) = -\boldsymbol{\Gamma}^0 * \boldsymbol{\tau}(\mathbf{x}) \quad \forall \mathbf{x} \in V, \quad \text{or} \quad \hat{\boldsymbol{\varepsilon}}(\boldsymbol{\xi}) = -\hat{\boldsymbol{\Gamma}}^0(\boldsymbol{\xi}) : \hat{\boldsymbol{\tau}}(\boldsymbol{\xi}) \;\; \forall \boldsymbol{\xi} \neq 0,\; \hat{\boldsymbol{\varepsilon}}(0) = \mathbf{0}$$

The operator $\boldsymbol{\Gamma}^0$ is explicitely known in Fourier space and, when the reference material is isotropic (with Lamé coefficients λ^0 et μ^0), takes the form:

$$\hat{\Gamma}^0_{ijkh}(\boldsymbol{\xi}) = \frac{1}{4\mu^0|\boldsymbol{\xi}|^2}(\delta_{ki}\xi_h\xi_j + \delta_{hi}\xi_k\xi_j + \delta_{kj}\xi_h\xi_i + \delta_{hj}\xi_k\xi_i) - \frac{\lambda^0+\mu^0}{\mu^0(\lambda^0+2\mu^0)}\frac{\xi_i\xi_j\xi_k\xi_h}{|\boldsymbol{\xi}|^4}.$$

1.3. THE LIPPMANN-SCHWINGER EQUATION.

The preliminary problem can be used to solve the problem of an inhomogeneous elastic composite material with stiffness $\mathbf{c}(\mathbf{x})$ at point $\mathbf{x}$ under prescribed strain $\mathbf{E}$. For simplicity $\mathbf{E}$ is assumed to be prescribed, although other average conditions could be considered as well (prescribed stresses).

$$\left.\begin{aligned} \boldsymbol{\sigma}(\mathbf{x}) &= \mathbf{c}(\mathbf{x}) : \left(\boldsymbol{\varepsilon}(\mathbf{u}^*(\mathbf{x})) + \mathbf{E}\right) \quad \forall \mathbf{x} \in V \\ \mathbf{div}\boldsymbol{\sigma}(\mathbf{x}) &= \mathbf{0} \quad \forall \mathbf{x} \in V, \quad \mathbf{u}^* \ \#, \ \boldsymbol{\sigma}.\mathbf{n} \ - \# \end{aligned}\right\} \tag{1.2}$$

A reference material $\mathbf{c}^0$ is introduced and a polarization tensor $\boldsymbol{\tau}(x)$, which is unknown a priori, is defined as

$$\boldsymbol{\tau}(\mathbf{x}) = \boldsymbol{\delta}\mathbf{c}(\mathbf{x}) : \boldsymbol{\varepsilon}(\mathbf{u}(\mathbf{x})), \quad \boldsymbol{\delta}\mathbf{c}(\mathbf{x}) \ = \ \mathbf{c}(\mathbf{x}) - \mathbf{c}^0. \tag{1.3}$$

Thus, the problem reduces to the *periodic Lippmann-Schwinger equation* (Kröner (1972)), which reads, in real space and Fourier space respectively:

$$\left.\begin{aligned} \boldsymbol{\varepsilon}(\mathbf{u}(\mathbf{x})) &= -\boldsymbol{\Gamma}^0(\mathbf{x}) * \boldsymbol{\tau}(\mathbf{x}) + \mathbf{E}, \\ \widehat{\boldsymbol{\varepsilon}}(\boldsymbol{\xi}) &= -\widehat{\boldsymbol{\Gamma}}^0(\boldsymbol{\xi}) : \widehat{\boldsymbol{\tau}}(\boldsymbol{\xi}) \quad \forall \boldsymbol{\xi} \neq \mathbf{0}, \quad \widehat{\boldsymbol{\varepsilon}}(\mathbf{0}) = \mathbf{E} \end{aligned}\right\} \tag{1.4}$$

where $\boldsymbol{\tau}$ is given by (1.3).

1.4. THE ALGORITHM.

The principle of the algorithm is to use alternately (1.3) and (1.4), in real space and Fourier space, respectively, in an iterative process, to solve (1.2):

$$\left.\begin{aligned} &\textit{Initialization}: \quad \boldsymbol{\varepsilon}^0(\mathbf{x}) = \mathbf{E}, \quad \forall \, \mathbf{x} \in V, \\ &\textit{Iterate } \mathrm{i}+1: \quad \boldsymbol{\varepsilon}^{\mathrm{i}} \text{ is known} \\ &\quad a) \ \boldsymbol{\sigma}^{\mathrm{i}}(\mathbf{x}) = \mathbf{c}(\mathbf{x}) : \boldsymbol{\varepsilon}^{\mathrm{i}}(\mathbf{x}). \text{ Convergence test} \\ &\quad b) \ \boldsymbol{\tau}^{\mathrm{i}}(\mathbf{x}) = \boldsymbol{\sigma}^{\mathrm{i}}(\mathbf{x}) - \mathbf{c}^0 : \boldsymbol{\varepsilon}^{\mathrm{i}}(\mathbf{x}), \\ &\quad c) \ \widehat{\boldsymbol{\tau}}^{\mathrm{i}} = \mathcal{F}(\boldsymbol{\tau}^{\mathrm{i}}), \\ &\quad d) \ \widehat{\boldsymbol{\varepsilon}}^{\mathrm{i}+1}(\boldsymbol{\xi}) = -\widehat{\boldsymbol{\Gamma}}^0(\boldsymbol{\xi}) : \widehat{\boldsymbol{\tau}}^{\mathrm{i}}(\boldsymbol{\xi}) \ \forall \boldsymbol{\xi} \neq \mathbf{0} \text{ and } \widehat{\boldsymbol{\varepsilon}}^{\mathrm{i}+1}(\mathbf{0}) = \mathbf{E}, \\ &\quad e) \ \boldsymbol{\varepsilon}^{\mathrm{i}+1} = \mathcal{F}^{-1}(\widehat{\boldsymbol{\varepsilon}}^{\mathrm{i}}) \end{aligned}\right\} \tag{1.5}$$

where $\mathcal{F}$ and $\mathcal{F}^{-1}$ denote the Fourier transform and the inverse Fourier transform.

The rate of convergence of the algorithm is governed by the choice of Lamé coefficients of the reference material. A good convergence rate was observed when λ^0 and μ^0 were prescribed to be the half sum of the minimum and maximum value of these coefficients in the composite (Moulinec and Suquet (1994)).

1.5. NONLINEAR BEHAVIOR.

The algorithm can be extended to the case where the individual constituents obey an incremental law (infinitesimal strains), *e.g.* phases with an elastic-plastic behavior with isotropic hardening. The loading is applied step by step. At each

loading step n, the overall strain $\mathbf{E}_n$ is prescribed, and the local problem is solved for $(\boldsymbol{\sigma}_n,\ \boldsymbol{\varepsilon}_n,\ p_n)$ via the procedure summarized below:

$$\left.\begin{array}{ll} & \textit{Iterate } i+1: \qquad \boldsymbol{\varepsilon}_n^i \text{ is known} \\ a) & \textit{Compute } \boldsymbol{\sigma}_n^i \textit{ and } p_n^i \textit{ from } (\boldsymbol{\varepsilon}_n^i,\ \boldsymbol{\sigma}_{n-1},\ \boldsymbol{\varepsilon}_{n-1},\ p_{n-1}) \\ & \text{Convergence test} \\ b) & \boldsymbol{\tau}_n^i(\mathbf{x}) = \boldsymbol{\sigma}_n^i(\mathbf{x}) - \mathbf{c}^0 : \boldsymbol{\varepsilon}_n^i(\mathbf{x}), \\ c) & \widehat{\boldsymbol{\tau}}_n^i = \mathcal{F}(\boldsymbol{\tau}_n^i), \\ d) & \widehat{\boldsymbol{\varepsilon}}_n^{i+1}(\boldsymbol{\xi}) = -\widehat{\boldsymbol{\Gamma}}^0(\boldsymbol{\xi}) : \widehat{\boldsymbol{\tau}}_n^i(\boldsymbol{\xi})\ \forall \boldsymbol{\xi} \neq \mathbf{0} \text{ and } \widehat{\boldsymbol{\varepsilon}}_n^{i+1}(\mathbf{0}) = \mathbf{E}, \\ e) & \boldsymbol{\varepsilon}_n^{i+1} = \mathcal{F}^{-1}(\widehat{\boldsymbol{\varepsilon}}_n^i) \end{array}\right\} \qquad (1.6)$$

This procedure is similar to the one adopted in the linear elastic case. The main difference is due to the calculation of the stress field $\boldsymbol{\sigma}_n^i$ (step *(a)*).

2. Applications to unidirectional fiber reinforced composites

2.1. CONFIGURATIONS

The above numerical scheme was applied to predict the overall and local response of unidirectional fiber reinforced composites. Owing to the translation invariance along the axial direction (parallel to the unit vector $\mathbf{e}_3$), the geometry and the material properties of these composites are completely specified by the same data on a cross section in the plane $(\mathbf{e}_1, \mathbf{e}_2)$ transverse to the fibers' direction.

Several configurations were investigated. In all of them, the fibers cross sections were assumed to be impenetrable circular disks, with identical radii. In all the analyses presented below, the fiber volume fraction was 47.5% .

Random configurations. A prescribed number of identical impenetrable circular fibers were placed randomly in the unit cell. Fibers intersecting the boundary of the unit cell were treated modulo the periodic lattice, *i.e.* by moving the part of the fiber which would lie outside the unit cell to the opposite boundary (Figure 1a).

Standard configurations. Configurations which are classical in FEM modelling, namely circular fibers arranged at the nodes of a square or hexagonal lattice, were also considered (Figure 1b).

All calculations were performed under the *generalized plane strains* condition (Michel and Suquet (1993)).

2.2. CONSTITUTIVE BEHAVIOUR OF THE INDIVIDUAL PHASES

The individual phases are assumed to be isotropic and elastic plastic with isotropic hardening. More specifically, their elastic properties are given by a Young modulus E and a Poisson ratio ν (labelled by f or m for fibers and matrix respectively) and their plastic properties are governed by the flow rule and the Von Mises criterion with linear isotropic hardening,

$$\sigma_{eq} = \sigma_0 + H\, p,$$

where σ_0 is the initial flow stress ($\sigma_0 = +\infty$ when the phase is purely elastic), H is the hardening modulus ($H = 0$ when the phase is ideally plastic), p is the equivalent plastic strain. This general form is specialized below to several cases: isotropic linear elastic fibers in an elastic-ideally plastic matrix (section 3), isotropic linear elastic fibers in an elastic plastic matrix with isotropic linear hardening (section 3), elastic-ideally plastic matrix and fibers with different flow stresses (section 4). The specific values of the material constants are given in each section.

3. Uniaxial transverse tension

The use of generalized plane strains allows to follow arbitrary paths in the space of macroscopic stresses. In this section monotone uniaxial tension in a transverse direction is considered. Fibers are assumed to be purely elastic and the matrix is a Von Mises material

$$E^f = 400\,000\ MPa, \quad \nu^f = 0.23,$$

$$E^m = 68\,900\ MPa, \quad \nu^m = 0.35, \quad \sigma_0^m = 68.9\ MPa.$$

The hardening modulus of the matrix is either $H^m = 0$ (ideally plastic case) or $H^m = 1\,710$ MPa (hardening case).

23 images at a spatial resolution of 1024 x 1024 points containing 64 fibers with a constant volume fraction (0.475) were considered. The choice of this spatial resolution (for a given number of fibers) stems from a study of the influence of spatial resolution on the accuracy of the results (reported elsewhere). The square and hexagonal configurations were also considered.

A uniaxial tension in the 0^0 direction was applied to each "random" configuration. The square and hexagonal configurations were submitted to a uniaxial tension at 0^0 and 45^0. The results are shown in Figure 2 (the average of the strain/stress response of the random configurations is the thick solid line) and summarized in Table 1.

Table 1. Uniaxial tension in the transverse plane.

Transverse Young modulus E_T^{hom}, flow stress σ_0^{hom} (ideally plastic matrix), hardening modulus H^{hom} (hardening matrix). Sample mean (s. mean) and sample standard deviations (ssd) over 23 random configurations (the sample standard deviations are expressed in percentage of the sample means of the corresponding constants). Hexagonal and square lattice.

	Random config.		Hexag. lattice		Square lattice	
Constant	*s. mean*	*ssd*	0^0	45^0	0^0	45^0
E_T^{hom} (MPa)	143 166	0.93%	139 655	139 580	153 190	128 600
σ_0^{hom} (MPa)	88.85	2.42%	87.95	79.55	98.01	79.56
H^{hom} (MPa)	10 002	6.54%	7 100	7 420	13 400	4 760

Comments 1. The square lattice has a marked transverse anisotropy, strengthened by the nonlinear behavior, which gives raise to different responses when the direction of tension makes an angle of 0^0 or 45^0 with one of the axis of the square lattice.

The low flow stress in the diagonal direction (45^0) is due to the presence of a shear plane passing through the matrix. Indeed, when a plane of shear can be passed through the weakest phase of a composite, the shear strength of the composite is exactly the strength of the weakest phase (Drucker (1959)). In uniaxial tension in a direction inclined at 45^0 on this plane, the transverse flow stress of the same composite cannot exceed $2\sigma_0^m/\sqrt{3}$. This is the flow stress observed on Figure 2 and Table 1 ($2\sigma_0^m/\sqrt{3} \simeq 79.56 MPa$). In conclusion, except at low volume fractions, the square lattice should not be used to investigate the transverse properties of transversely isotropic nonlinear composites.

2. The hexagonal lattice approaches transverse isotropy. When the matrix is a hardening material, the predictions obtained with the hexagonal lattice underestimate the stiffness of the composite, or at least are located below the average of the predictions for the random configurations in the range of overall deformations considered. Another computation, not reported here, has been performed up to 30% of transverse strain, with no modification in the conclusions. A similar observation was made by Brockenborough *et al* (1991) on another system. When the matrix is ideally plastic, the low flow stress in the diagonal direction (45^0) is again due to the presence of a shear plane passing through the matrix. In conclusion, the hexagonal lattice should be used with care to predict the transverse properties of nonlinear composite systems, even for hardening matrices.

3. The deviation from the average of the transverse Young's moduli computed on the different configurations is small. By contrast, the deviations in the other properties (flow stress, hardening modulus) are higher and might probably be attributed to the combined effects of nonlinearity and incompressibility.

4. The inspection of the local plastic strains reveals significant differences between the ideally plastic case and the hardening case. When the matrix is ideally plastic, the strain localizes in thin bands in the matrix. In most configurations, only a small percentage of the matrix contributes to the plastic dissipation. The overall flow stress of the composite is observed to be in direct relation with the "tortuosity" of these bands. This observation is consistent with Drucker's remark and one of the most meaningful geometrical parameter seems to be the length of the shortest path passing through the matrix at an angle of approximately 45^0 (in tension, or 0^0 in shear). When the matrix is a hardening material, the plastic strain spreads all over the matrix. The whole matrix contributes (although non homogeneously) to the plastic dissipation and, consequently, to the overall strengthening of the composite. In spite of these differences, it has been observed that the "stiffest" (respectively the "weakest") configurations in the ideally plastic case remain the stiffest (respectively the weakest) configurations in the hardening case.

4. Overall flow surface of unidirectional composites

4.1. OVERALL FLOW SURFACE

When the macroscopic stress state $\mathbf{\Sigma}$ is multiaxial instead of being uniaxial, the notion of *overall flow stress* can be generalized into the notion of *overall flow surface*

of the composite. First, the *overall strength domain* of the composite is defined as the domain of overall stress states $\boldsymbol{\Sigma}$ which can be associated to a local stress field $\boldsymbol{\sigma}$ which is both in equilibrium with $\boldsymbol{\Sigma}$ and satisfies the strength condition (Suquet (1983) (1987)):

$$P^{hom} = \{\boldsymbol{\Sigma} \in \mathbb{R}^{3\times 3}_s, \text{ such that there exists } \boldsymbol{\sigma}(\mathbf{x}) \text{ with } \langle\boldsymbol{\sigma}\rangle = \boldsymbol{\Sigma},$$
$$\mathbf{div}(\boldsymbol{\sigma}(\mathbf{x})) = \mathbf{0},\ \sigma_{eq}(\mathbf{x}) \leq \sigma_0(\mathbf{x}),\ \text{for every } \mathbf{x} \text{ in } V\}.$$

The *overall flow surface of the composite* (or its *extremal surface* according to Hill (1967)) is the boundary of P^{hom}. It depends on the flow stress of each phase, on their volume fractions and on their arrangement but is independent of the behavior of its individual constituents prior to the flow stress.

The general properties of P^{hom} will not be discussed here (the interested reader is referred to Suquet (1983) (1987)). We limit our attention to the numerical calculation of P^{hom} in two-phase materials with two different flow stresses, one phase being under the form of cylindrical fibers with a circular cross section dispersed into the other phase. The boundary of P^{hom} is determined according to a procedure described in Marigo *et al* (1987) and Michel and Suquet (1993). In this procedure, each individual phase is assumed to be given an elastic ideally plastic behaviour and, for a prescribed radial direction in the space of stress, the response of the composite along this direction of loading is computed. The overall stress reaches an asymptotic value which is on the extremal surface.

The overall stresses under consideration consist of the superposition of a uniaxial tension and a transverse shear (this example was first considered by Ponte Castañeda and De Botton (1992))

$$\boldsymbol{\Sigma} = \Sigma_1\,(\mathbf{e}_1 \otimes \mathbf{e}_1 - \mathbf{e}_2 \otimes \mathbf{e}_2) + \Sigma_3\ \mathbf{e}_3 \otimes \mathbf{e}_3.$$

The extremal yield surface lies in the plane (Σ_1, Σ_3).

4.2. NUMERICAL SIMULATIONS

Three contrast ratios between the strengths of the two phases σ_0^f/σ_0^m have been investigated: $\sigma_0^f/\sigma_0^m = 2,\ 5,\ 10$. For one of them, $\sigma_0^f/\sigma_0^m = 2$, the computations were performed with 11 of the 23 configurations used in section 3. For the other two ratios, the computations were performed one a single configuration representative of the average of the predictions over the whole set of configurations, when $\sigma_0^f/\sigma_0^m = 2$. More specifically this configuration approaches transverse isotropy and its overall strain/stress response is close to the mean response of all the configurations - as well under multiaxial loading, as under uniaxial tension. The results are shown in Figure 3 and summarized in Table 2.

In all three cases, the shape of the extremal surface ressembles a bimodal surface. Bimodal surfaces have been used by Hashin (1980), Dvorak (1988), De Buhan and Taliercio (1991), Ponte Castañeda and De Botton (1992) and several other authors to describe the first yield or the flow surface of unidirectional composites. The present calculations confirm the validity of this assumption or observation.

The inspection of the failure modes at the local level reveals that the unit cell can fail under two possible modes and confirms even further the bimodal shape of the overall flow surface. The first mode, observable for low values of the axial stress Σ_3, corresponds to shear bands in the matrix with an inclination of approximately $\pm 45^0$ on the horizontal direction. When Σ_3 reaches a threshold corresponding to the vertex of the flow surface, the plastic zone spreads throughout the unit cell. As Σ_3 is increased, the plastic strain tends to be more and more homogeneous and becomes fully homogeneous when Σ_3 reaches $< \sigma_0 >$ (Figure 4).

These numerical calculations can be used to propose a closed form expression to the bimodal surface. Indeed, simple piecewise constant stress fields meeting both the requirements of equilibrium and of strength can be constructed and lead to the following **inner** approximation of P^{hom}

$$|\Sigma_3| \leq v_f \left((\sigma_0^f)^2 - 3\Sigma_1^2\right)^{1/2} + v_m \left((\sigma_0^m)^2 - 3\Sigma_1^2\right)^{1/2}. \tag{4.1}$$

The strength in shear predicted by (4.1) coincides with the strength in shear of the matrix, $\sigma_0^m/\sqrt{3}$, while the calculations show a small increase in strength due to the fibers. This increase can be taken into account by modifying (4.1) into

$$|\Sigma_3| \leq v_f \left((\sigma_0^f)^2 - 3\Sigma_1^2\right)^{1/2} + v_m \left((\sigma_0^m)^2 - (\frac{\sigma_0^m}{k_*}\Sigma_1)^2\right)^{1/2} \tag{4.2}$$

k_*, in-plane shear strength of the composite, is the only adjustable parameter contained in (4.2). The resulting simple expression (4.2), with k_* adjusted in pure in-plane shear, fits well with the results of numerical calculations performed on radial paths with arbitrary orientation.

Table 2. Overall flow surface under combined axial tension and in plane shear.

$\sigma_0^f/\sigma_0^m = 2$		$\sigma_0^f/\sigma_0^m = 5$		$\sigma_0^f/\sigma_0^m = 10$	
Σ_1/σ_0^m	Σ_3/σ_0^m	Σ_1/σ_0^m	Σ_3/σ_0^m	Σ_1/σ_0^m	Σ_3/σ_0^m
0.626	0.000	0.638	0.000	0.640	0.000
0.626	0.626	0.639	1.756	0.642	3.640
0.616	0.879	0.637	2.379	0.642	4.053
0.580	1.005	0.591	2.562	0.642	4.569
0.448	1.231	0.478	2.709	0.638	4.850
0.356	1.328	0.391	2.779	0.609	4.963
0.201	1.430	0.250	2.853	0.533	5.072
0.000	1.475	0.000	2.900	0.450	5.142
*	*	*	*	0.184	5.255
*	*	*	*	0.000	5.275

Acknowledgments.

This study is part of the "Eurhomogenization" project supported by the SCIENCE Program of the Commission of the European Communities under contract

ERB4002PL910092. Use of the supercomputer CRAY YMP at IMT was possible through a grant of the PACA region. Helpful discussions with J.C. Michel and P. Ponte Castañeda are gratefully acknowledged.

References.

Adams, D.F. and Doner, D.R. (1967) Tranverse normal loading of a unidirectional composite, *J. Comp. Mat.*, **1**, 152

Böhm, H.J., Rammerstoffer, F.G. and Weissenbeck,E. (1993) Some simple models for micromechanical investigations of fiber arrangements in MMCs, *Comput. Mat. Sc.*, **1**, 177-194.

Brockenborough, J.R., Suresh, S. and Wienecke, H.A. (1991) Deformation of Metal-Matrix Composites with continuous fibers: geometrical effects of fiber distribution and shape, *Acta Metall. Mater.*, **39**, 735-752.

Christman, T., Needleman, A. and Suresh, S. (1989) An experimental and numerical study of deformation in metal-ceramic composites, *Acta Metall. Mater.*, **37**, 3029-3050.

De Buhan, P. and Taliercio A. (1991) A homogenization approach to the yield strength of composite materials, *Eur. J. Mech. A/ Solids*, **10**, 129-150.

Drucker, D.C. (1959) On minimum weight design and strength of nonhomogeneous plastic bodies, in Olszak (ed.), *Nonhomogeneity in Elasticity and Plasticity*, Pergamon Press, 139-146.

Dvorak, G., Bahei-El-Din, Y.A., Macheret, Y. and Liu, C.H. (1988) An experimental study of elastic-plastic behavior of a fibrous Boron-Aluminum composite, *J. Mech. Phys. Solids*, **36**, 655-687.

Hashin, Z. (1980) Failure Criteria for Unidirectional Fiber Composites, *J. Appl. Mech.*, **47**, 329-334.

Hill, R. (1967) The essential structure of constitutive laws for metal composites and polycristals, *J. Mech. Phys. Solids*, **15**, 79-95.

Kröner, E. (1972) *Statistical Continuum Mechanics*, Springer Verlag, Wien, 117.

Marigo, J.J., Mialon, P., Michel J.C. and Suquet, P. (1987) Plasticité et homogénéisation : un exemple de prévision des charges limites d'une structure périodiquement hétérogène, *J. Méca. Th. Appl.*, **6**, 47-75.

Michel, J.C. and Suquet, P. (1993) On the strength of composite materials: variational bounds and numerical aspects, in M.P. Bendsoe, C. Mota-Soares (eds.), *Topology Design of Structures*, Kluwer Pub., Dordrecht pp. 355-374.

Moulinec, H. and Suquet, P. (1994) A fast numerical method for computing the linear and nonlinear properties of composites *C. R. Acad. Sc. Paris*, II, **318**, 1417-1423.

Nakamura, T. and Suresh, S. (1993) Effects of thermal residual stresses and fiber packing on deformation of metal-matrix composites, *Acta metall. mater.*, **41**, 1665-1681.

Ponte Castañeda, P. (1992) New variational principles in Plasticity and their application to composite materials, *J. Mech. Phys. Solids*, **40**, 1757-1788.

Ponte Castañeda, P. and De Botton, G. (1992) On the homogenized yield strength of two-phase composites, *Proc. Royal Soc. London A*, **438**, 1992, 419-431.

Suquet, P. (1983) Analyse limite et homogénéisation, *C. R. Acad. Sc. Paris*, II, **296**, 1355-1358.

Suquet, P. (1987) Elements of Homogenization for Inelastic Solid Mechanics, in E. Sanchez Palencia and A. Zaoui (eds.) *Homogenization Techniques for Composite Media*, Lecture Notes in Physics $N^0$272, Springer-Verlag. Berlin, pp.193-278.

Suquet, P. (1993), Overall potentials and flow stresses of ideally plastic or power law materials, *J. Mech. Phys. Solids*, **41**, 981-1002.

Tvergaard, V. (1990) Analysis of tensile properties for a whisker–reinforced metal-matrix composite, *Acta Metall. Mater.*, **38**, 185-194.

Willis, J.R. (1991) On methods for bounding the overall properties of nonlinear composites, *J. Mech. Phys. Solids*, **39**, 73-86 and **40**, 441.

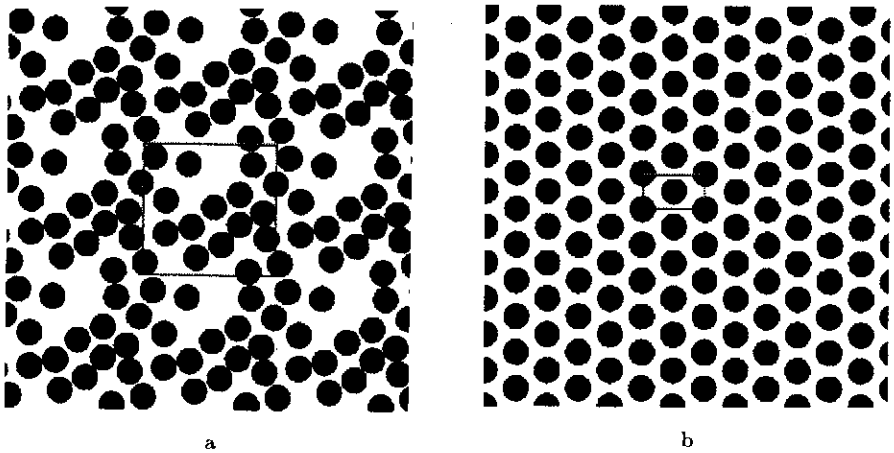

a b

Figure 1. Configurations.

Periodic unit cell (framed area) containing 16 identical circular fibers placed randomly (Fig. 1.a). Hexagonal lattice (Fig. 1.b). The unit cell (framed area) contains $1 + 4 \times \frac{1}{4} = 2$ fibers.

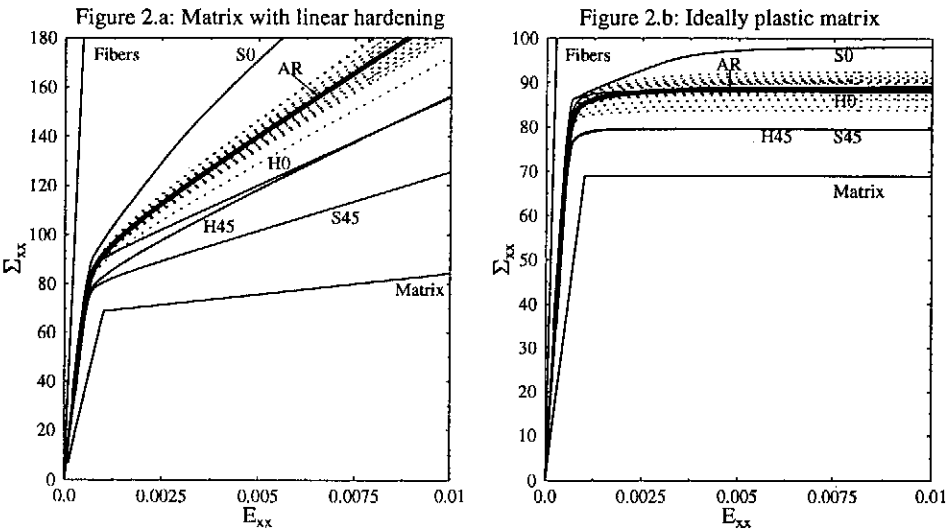

Figure 2. Uniaxial transverse tension.

Overall stress-strain response computed with the present method. Fibers volume fraction = 47.5%. Dotted lines: 23 configurations of 64 identical circular fibers placed randomly in the unit cell. Thick solid line: average of the random configurations (AR). S0 (resp. S45): fibers placed at the nodes of a square lattice, tension at 0° (resp. 45°). H0 (resp. H45): fibers placed at the nodes of a hexagonal lattice, tension at 0° (resp. 45°).

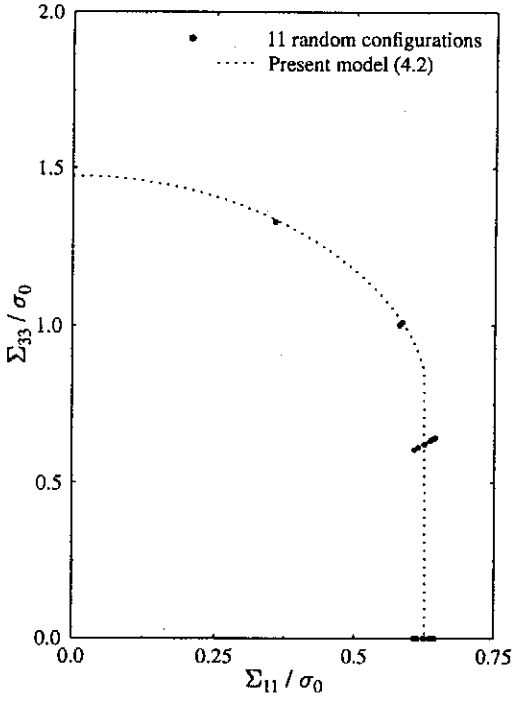

Figure 3. Overall flow surface of unidirectional composites.

Figure 3a: $\sigma_0^f/\sigma_0^m = 2$.

Numerical results for 11 random configurations (full circles).

Present model (4.2) (dotted line). The strength in shear k^* in (4.2) is computed on a representative configuration.

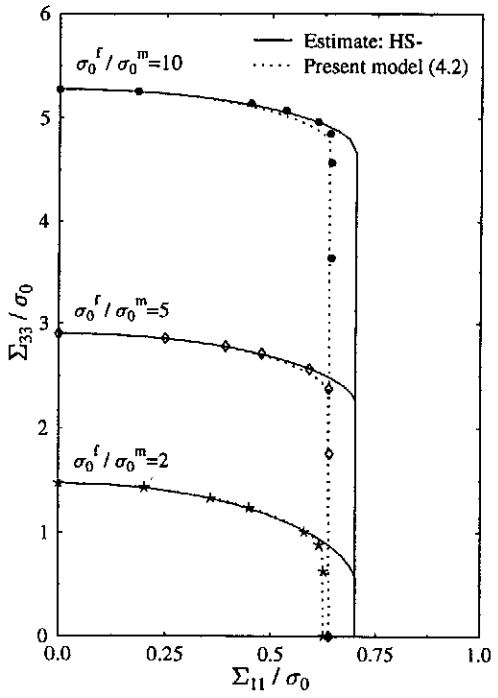

Figure 3b: Yield surface for a representative configuration.

- $*$: $\sigma_0^f/\sigma_0^m = 2$
- $\diamond$: $\sigma_0^f/\sigma_0^m = 5$
- $\bullet$: $\sigma_0^f/\sigma_0^m = 10$

Present model (4.2) (dotted lines).

Prediction of nonlinear bounding theories (Ponte Castañeda and De Botton (1992), Suquet (1993)) using the lower Hashin-Shtrikman linear bound (solid line).

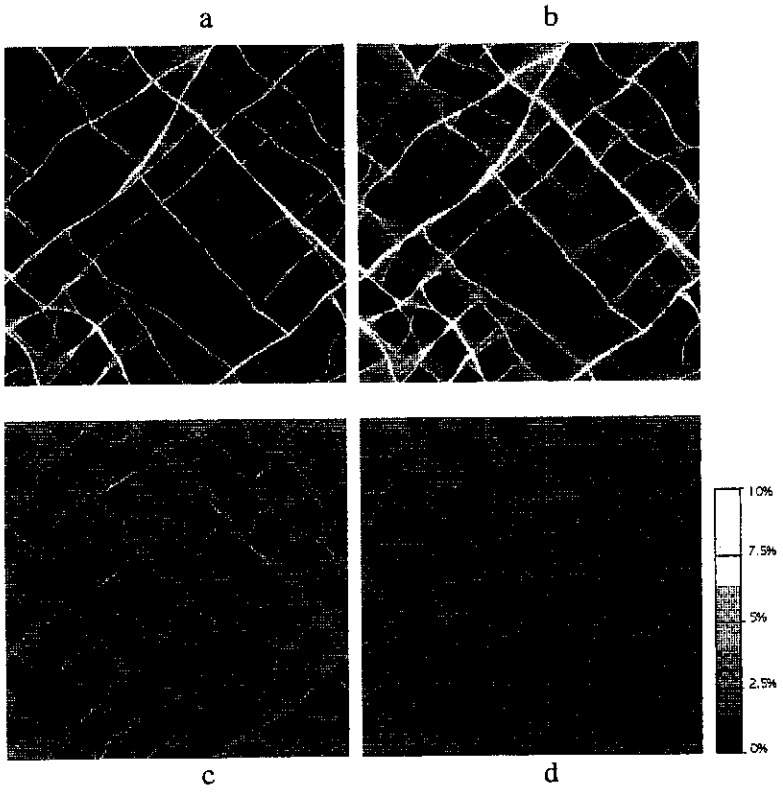

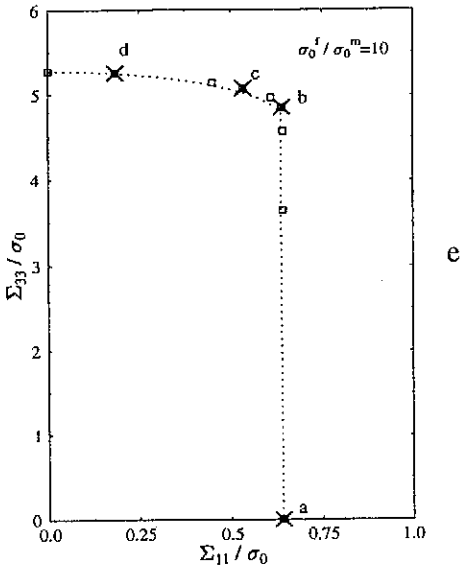

e

Figure 4. Overall flow surface.

Maps of the equivalent plastic strain in a composite reinforced by identical unidirectional circular fibers. Fibers volume fraction = 47.5%. $\sigma_0^f / \sigma_0^m = 10$. Loading conditions described in sect. 4.1.

Figure 4.a, 4.b, 4.c, and 4.d: equivalent plastic strains corresponding to 4 different extremal stresses (crosses a, b, c and d in figure 4.e). Overall strain in the direction of the applied stress= 1%.